Bridging the Gap Between Osmotic and Crystalline Swelling in Smectites Clays Minerals

Claire HOTTON[a], Thomas BIZIEN[b], Cyrille HAMON[a], Eric FERRAGE[c,*], Erwan PAINEAU[a,*]

[a] Université Paris-Saclay, CNRS, Laboratoire de Physique des Solides, Orsay, 91405, France
[b] Synchrotron SOLEIL, L'Orme des Merisiers, 91192 Gif-sur-Yvette Cedex, France
[c] Institut de Chimie des Milieux et Matériaux de Poitiers (IC2MP), Université de Poitiers, CNRS, Poitiers, 86073, France

* Corresponding authors:
erwan-nicolas.paineau-lanone@cnrs.fr. Phone: +33 (0) 1 69 15 60 51
eric.ferrage@univ-poitiers.fr

Abstract

The swelling behavior of smectite clay minerals has been extensively investigated due to their critical role in construction stability. Two distinct swelling regimes have long been recognized: crystalline swelling, involving the incorporation of a few water sheets between clay layers, and osmotic swelling, characterized by the complete delamination of individual clay layers. Crystalline swelling mechanisms have been well established through hydration techniques applied to dry clay in a humid environment, while osmotic swelling has been observed through the gradual concentration of a diluted clay suspension into a more compact, glassy state. Although a linear transition between these two regimes has been proposed, it has yet to be experimentally demonstrated. In this study, we investigate the complete dehydration process of a levitated smectite suspension droplet using in-situ Small Angle X-ray Scattering (SAXS). The results reveal a gradual shift from osmotic swelling to crystalline swelling, marked by a transition from a pure nematic glass to a coexistence zone where the nematic phase contracts and a saturated crystalline phase emerges, ultimately progressing to an unsaturated crystalline state. This transition occurs through a continuous process in which the interlayer space decreases from four water layers to zero water layers, forming stratified interlayers along the way.

Keywords: smectite, swelling, dehydration mechanism, phase transition, acoustic levitation, Small Angle X-ray Scattering

Introduction

Clay minerals are lamellar aluminosilicates, naturally present in most soils and used since early prehistoric times for their unique physical and chemical properties [1]. Among these properties, some clay minerals have the ability to accommodate water within their sheets, leading to significant swelling properties. These swelling clay minerals, such as the smectite group, are constituted by 2:1 (TOT) layer whose structure consists of a parallel stacking of one octahedral sheet (O) sandwiched between two tetrahedral sheets (T). The presence of isomorphic substitutions by cations of lower valency induces a permanent negative structural charge, either in the tetrahedral or in the octahedral sheet. This charge is compensated by cations present in the interlayer space with a charge per half unit cell ranging from 0.2 to 0.6 [2]. The swelling capacity of smectites then strongly depends on the solvation of these counterions, which is a direct result of their nature and their valency, as well as the ionic strength of the aqueous medium [3]. Swelling properties have been long recognized, arousing the interest not only of geologists but also of chemists, physicists and biologists from academia and industry due to their numerous industrial and environmental applications. Notably, swelling properties of smectites are used to predict the impact of soil modification due to moisture on constructions, for their use as barriers for the disposal of industrial or nuclear wastes or as additives in drilling mud in the petroleum industry [4,5].

The swelling of smectites is divided into two main regimes most often qualified as crystalline and osmotic swellings [6–8]. The layer-to-layer distance for smectites at the dry state (0W layer) is around 10 Å. Since the pioneer works of Bradley et al. (1937), the crystalline swelling corresponds to a 1D expansion of the clay layer-to-layer distance by incorporation of water sheets into the interlayer space [9]. It is now well-established that the interlayer space can incorporate several water sheets, increasing the layer-to-layer distance to 12.3-12.7 Å for one (1W), 15.2-15.8 Å for two (2W) and 18.0-19 Å for three sheets of water (3W) depending on the nature of the interlayer cation (size, valency) [10–14]. The possibility of a 4W hydration state with layer-to-layer distance of 21.4-22 Å has been reported since the forties but remains rarely observed, only in systems of montmorillonite samples (low-charged smectite with octahedral layer charge) [7,15,16]. The second regime is the so-called osmotic swelling, which occurs at higher water content. This state corresponds to a complete delamination of the material into individual platelets, typically by

dispersing powder samples into ultrapure water [17,18]. When the water content is increased, there is a difference in ion concentration between the interlayer space and the bulk water, resulting in the formation of an osmotic pressure gradient and a reduction of the platelets cohesion [19]. In addition, the cations present in the interlayer space are hydrated and therefore mobile, meaning that water molecules can penetrate the interlayer space to balance the difference in osmotic pressure. The osmotic swelling is possible only for low bonding energy cations, i.e., in the case of smectites homoionized with monovalent cations such as Li^+ or Na^+ [7,20]. The layer-to-layer distance increases until the platelets are fully dispersed, forming colloidal sols whose stability is governed by the Derjaguin-Landau-Verwey-Overbeek (DLVO) theory, with the range of electrostatic interactions defined by the Debye length. The colloidal stability of smectites has also been extensively studied theoretically, with numerous models proposed to explain particle organization in the dilute regime (3D osmotic swelling). In this regime, the system initially exhibits an isotropic phase, which may transition into a nematic liquid crystal phase before evolving into an arrested state with nematic-like ordering (1D osmotic swelling), typically occurring at volume fractions of a few percent.

To probe the structure evolution, the most appropriate approach is to perform time resolved small-angle X-ray (SAXS) or neutron scattering experiments [21–23] during hydration or drying. Smectites have been studied through two distinct approaches, either by adding water to the system or by removing it. As early as 1954, Norrish [7] suggested a linear evolution between these two regimes. However, this fundamental question has never been explored experimentally so far owing to the difficulty in investigating the transition between fully dispersed and fully dry nanosheet states through a single experiment. We propose here a novel strategy to study the swelling of clay minerals, revealing the transition from fully dispersed to fully dried smectite platelets by continuous evaporation. Among recent developments, acoustic levitation [24,25] emerges as an effective approach for conducting in-situ studies on self-standing droplets, enabling real-time kinetic analysis. The immobilization of droplets at the nodes of an acoustic standing wave, can be experimentally achieved between an ultrasonic transducer and a reflector [26,27]. The combination of SAXS with acoustic levitation can address a variety of scientific challenges, including the investigation of the self-assembly of colloids or proteins [28–30], out-of-equilibrium phenomena and revisiting phase diagrams [31].

In this study, the dehydration process of a levitated droplet of smectite suspensions is investigated using time-resolved Small Angle X-ray Scattering coupled with an acoustic levitator (LevSAXS). In this configuration, we have been able to fully capture the evolution of layer-to-layer distances from the dilute regime (isotropic/nematic transition and liquid/glass transition) to the concentrated crystalline regime and ultimately the dry state. Notably, this investigation reveals the gradual transition from osmotic to crystalline swelling, defining the various hydration states of smectites, details the evolution of layer-to-layer distances, the relative proportions of platelets involved in each process, and the transitions between these states.

Results

Osmotic swelling regime

We selected a standard beidellite from Idaho (SBId-1, i.e., low-charged smectite with tetrahedral layer charge), which is known to display a rich colloidal behaviour in dilute conditions with a transition from isotropic to nematic liquid-crystalline phase before forming an arrested phase for ϕ ~ 1% [32]. Before use, the clay sample is purified of accessory minerals and Na-saturated according to previously established procedure [33,34]. Then, a size fractionation is applied by successive centrifugation at various speed and redispersion in ultrapure water, resulting in a dispersion of discoidal particles with a mean diameter of 210 nm (polydispersity of 38%) and an average thickness of 0.6 nm [32]. The volume fraction (ϕ) of nanosheets is adjusted by dilution of a concentrated stock solution obtained by osmotic stress [35].

Upon evaporation of a diluted smectite suspension, the system first evolves through the 3D osmotic swelling regime, followed by an 1D crystalline compression until the dry state. During the osmotic swelling regime, liquid-crystalline phase may appear. Indeed, suspensions of plate like particles can exhibit liquid-crystalline phase transition depending on the aspect ratio as volume fraction increases due to a competition between orientational entropy and packing entropy governed by excluded volume interactions [36–38]. At thermodynamic equilibrium, beidellite suspension exhibit an isotropic/nematic (I/N) transition in the liquid state [32,39]. Above a critical volume fraction, the platelets show rotational and translational arrested motion into a glass-like state displaying a nematic-like ordering. The observation of such phases is typically observed after long

equilibration time in capillaries whereas during evaporation the system may be out of equilibrium, possibly impacting these transitions.

We first assessed phase transition during evaporation process using LevSAXS set-up (**Figure 1**).

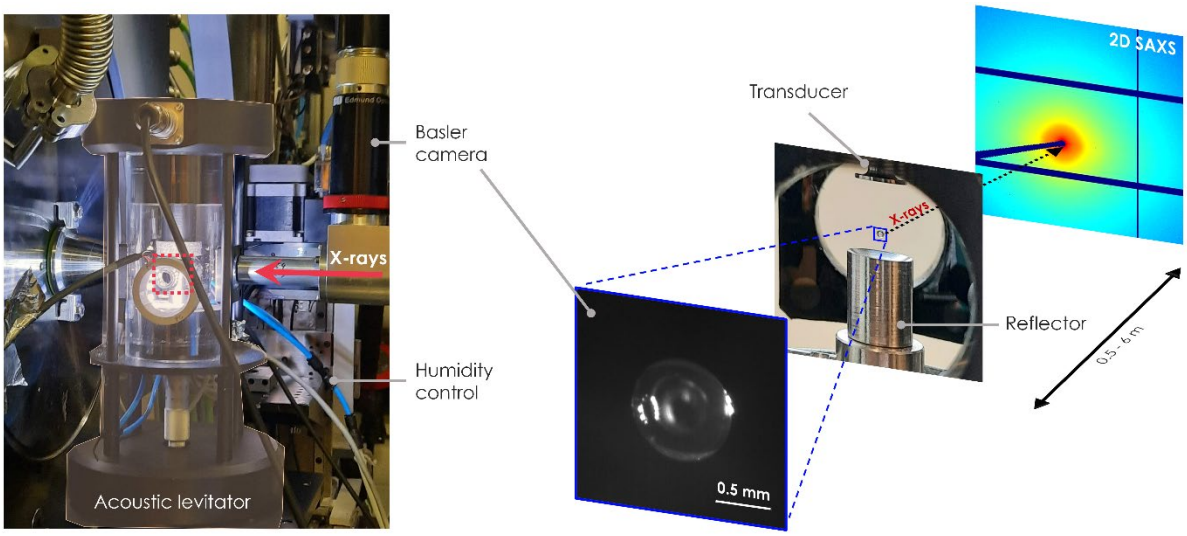

Figure 1. LevSAXS set-up including the acoustic levitator implemented on the SAXS beamline (SWING, Synchrotron SOLEIL). Zoom in on the levitated droplet between the transducer and the reflector with the corresponding image on the Basler camera.

In-situ LevSAXS measurements have been performed every second troughs the levitated droplet under controlled humidity, and the volume fraction over time was determined from image analysis of the droplet recorded with a Basler camera. We have performed the experiment with three different initial concentrations: $\phi_{initial}$ = 0.1%, 0.4% and 0.55% at 70% of relative humidity.

At $\phi_{initial}$ = 0.1%, the SAXS curves on **Figure 2A and Figure S1A** present a monotonous decay of the scattered intensity I with scattering vector Q, that scales as $I(q) \sim Q^{-2}$ and the 2D SAXS images are isotropic (**Video S1**). This feature is characteristic of the form factor of the 2D platelet, describing well the light scattering of an isotropic state where particles are noninteracting and present a free motion. At a certain stage of evaporation (ϕ = 1%, 866s), the SAXS patterns display periodic oscillations with Q-value following 1:2:3 progression as well as anisotropic 2D SAXS images, showing two facing circle arcs at higher volume fraction, characteristic of the presence of a nematic phase (**Video S1**). The average interparticle distance can be estimated from the position of the first maximum as: $d \approx (2\pi)/(q_{max})$. It appears that the I/N transition occurs at an interparticle distance of 58.5 nm, corresponding to a volume fraction of 1%, i.e. to the glass state at thermodynamic equilibrium. So far, there is no evidence of a I/N transition in the liquid state.

The same experiment was then conducted with initial volume fractions ($\phi_{initial}$) of 0.4% and 0.55%, which display a combination of isotropic and biphasic states or only biphasic states respectively. This organization was also seen in levSAXS. For $\phi_{initial}$=0.4%, the levSAXS patterns were isotropic, showing a broad modulation in scattered intensity due to the short-range positional, or "liquid-like", order of the platelets, indicative of the isotropic state (**Figures 2B and S1B, Video S2**). At $\phi_{initial}$=0.55%, however, the SAXS patterns were anisotropic, displaying periodic oscillations with Q-values in a 1:2:3 sequence, characteristic of a liquid nematic phase (**Figure 2C and S1C, Video S3**). In both cases, a transition occurred upon drying around 0.9%, as shown by integrating parts of the SAXS images (**Figure 2D**, **Figure S2**). This revealed two distinct structural organizations within the droplets. For instance, at 1.06% (515s) there is a first broad peak at 0.01 $Å^{-1}$ corresponding to a distance of 62.8 nm and a series of 3 peaks following a 1:2:3 progression with the first peak at 0.0136 $Å^{-1}$ corresponding to a distance of 46.1 nm (**Figure 2D**). This can be due to a heterogeneous distribution of the platelets inside the droplet at a certain stage of drying. Indeed, the evaporation time is large compared to the diffusion of the particles inside the droplet, leading to a Péclet number Pe >> 1 and thus to a preferential organization of the platelets at the interface of the droplet during drying. This distinguishes the face-to-face platelets stacking at the interface with a smaller inter-particle distance from the "bulk" at the center of the droplet with larger inter-particle distances. From 1.12% (632s, interparticle distance of 55.5 nm), the SAXS patterns display periodic oscillations as well as anisotropic 2D SAXS images showing two facing circle arcs or dots (**Video S2**), characteristic of the presence of a nematic glass. Overall, regardless of the initial volume fraction, the system appears to undergo a transition around 1%, either evolving into a nematic glass or forming a biphasic system. The variation in phase transitions depending on the initial volume fraction is probably due to constant mixing within the droplet, driven by acoustic pressure forces, which prevents the formation of the liquid nematic phase.

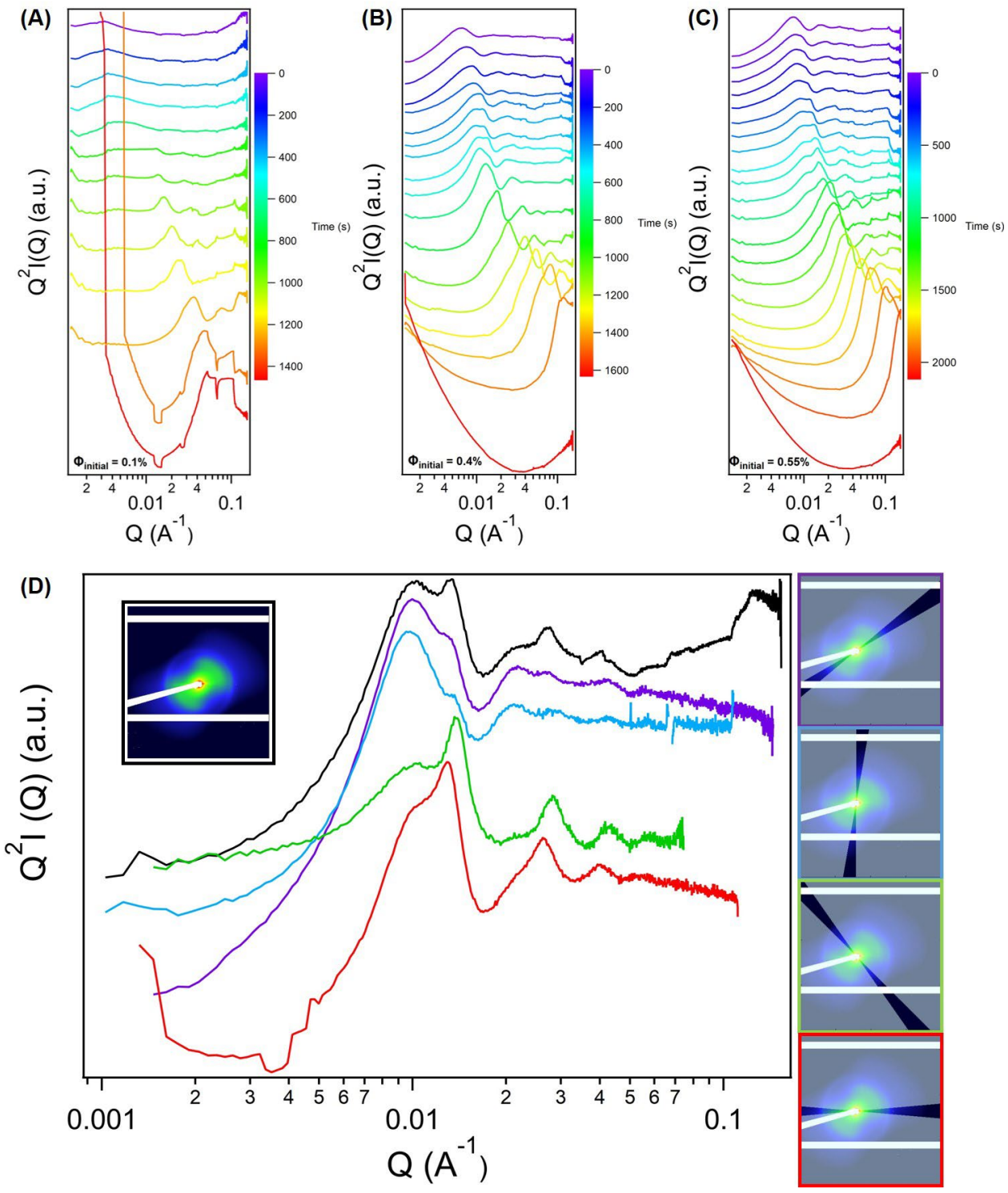

Figure 2. Structures factors $Q^2I(Q)$ as a function of the scattering vectors Q and as a function of time for 1 µL droplet of SBId-1 (**(A)** $\Phi_{initial}$ = 0.1%, **(B)** $\Phi_{initial}$ = 0.4%, and **(C)** $\Phi_{initial}$ = 0.55%) dried under acoustic levitation at 70% of relative humidity. The figures show only a few curves of the evaporation process for the sake of clarity; all the curves are shown in **Figure S1**. The curves

have been shifted vertically for the sake of clarity. **(D)** Structures factors $Q^2I(Q)$ as a function of the scattering vectors Q of SBId-1 ($\Phi_{initial}$ = 0.4%) at 515s (Φ_{515s} = 1.06%) during drying under acoustic levitation at 70% of relative humidity. The black curve is obtained through a radial integration of the corresponding 2D SAXS images circled in black. The colored curves are obtained through partial radial integration of the corresponding 2D SAXS images circled in the corresponding color. The curves have been shifted vertically for the sake of the clarity.

From these levSAXS patterns, we can extract the swelling law relating the evolution of the average interparticle distance as a function of the volume fraction. **Figure 3** presents the corresponding swelling laws of beidellite during evaporation for the different initial volume fraction. All data point scale on a master curve, whose slope evolves as ϕ^{-1}, reflecting a local lamellar order of the beidellite platelets. This trend is characteristic of most smectites [17,40], as demonstrated in **Figure 3**, which presents measurements on capillaries of various smectite suspensions concentrated by osmotic stress [32]. In the region of high-volume fraction, the ϕ^{-1} dependence on interparticle distance diverges, likely due to concentration heterogeneities of particles within the droplet during the drying process. At thermodynamic equilibrium, the swelling laws at low volume fractions show a $\phi^{-1/3}$ dependence with the interparticle distance characteristic of the 3D swelling of the noninteracting platelets. This regime is not observed by acoustic levitation probably due to the constant mixing within the droplet driven by acoustic pressure forces.

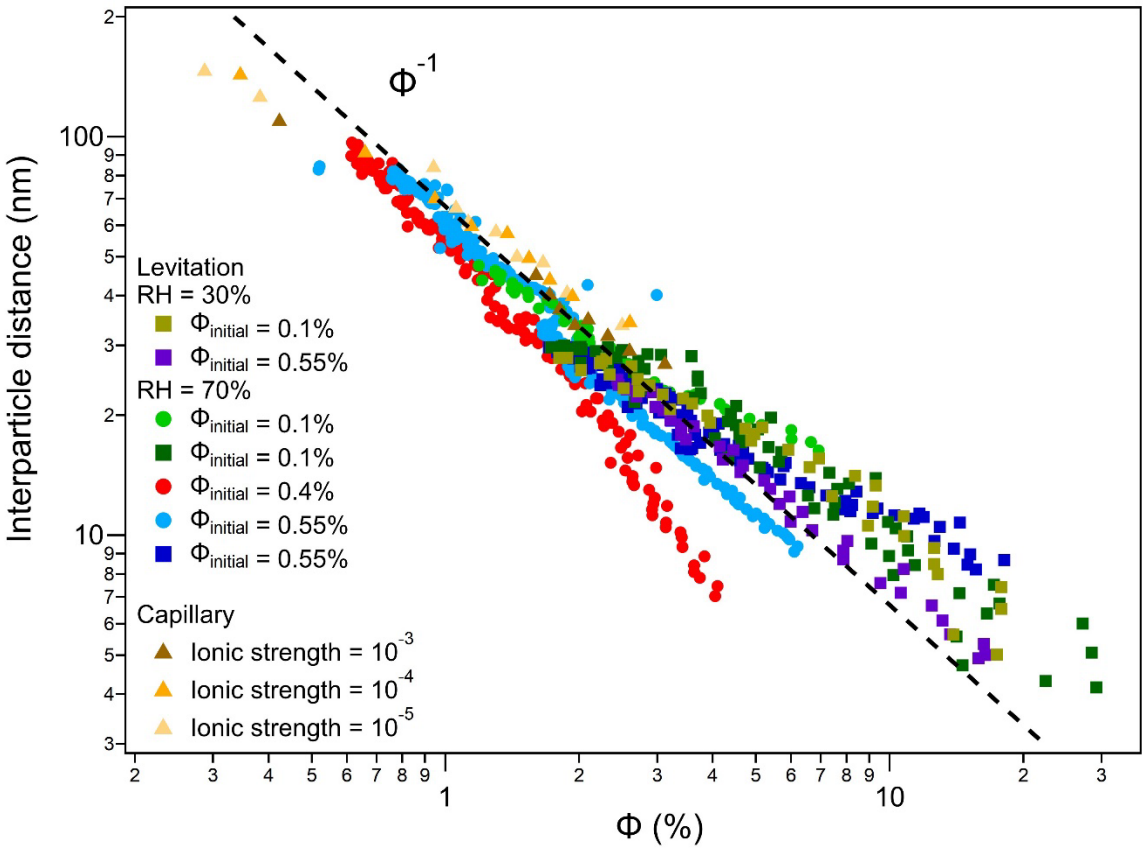

Figure 3. Evolution of the interparticle distance deduced from SAXS (round symbols) and WAXS (square symbols) curves as a function of SBId-1 volume fraction. The dotted line corresponds to the dependence of the interparticle distance as a function of ϕ^{-1}. Evolution of the interparticle distance deduced from SAXS measurements on capillaries of various smectite suspensions concentrated by osmotic stress at various ionic strength from [32] are added for comparison.

Crystalline swelling

As the system dries, the layer-to-layer distance decreases, shifting the nematic peak towards higher Q-values. At a certain stage, clearly defined diffraction peaks appear on the SAXS curves in addition to the characteristic nematic glass pattern (**Figure 4A** and **Figures S3, Videos S4-S5**). This corresponds to the crystalline compression, i.e., face-to-face stacks of clay layers with water sheets in between. Before reaching the complete dry state (i.e., 0W layer, with a layer-to-layer distance of ~10 Å), the system undergoes a dehydration process marked by complex transitions, with the presence of different discrete hydration states.

For all initial volume fractions investigated (**Figure 4B-E** and **Figure S4**), 001 reflections of typical 4W (~ 20.8 Å) and 3W (~ 18.2 Å) hydration states appears in addition to the broad nematic peak, quickly followed by the appearance of a peak corresponding to 2W layers (~ 15.1 Å). We observe the coexistence of these three different hydration states for a few seconds followed by the disappearance of the 4W peaks and the coexistence of the 3W and 2W hydration states. At the end of the drying process, we only have the presence of the 2W layers reflection. It has already been shown that the crystalline dehydration is a continuous process due to layer charge heterogeneities, leading to the coexistence of layers with clay layers having different hydration states in the same crystal, leading to the so-called mixed-layer structures [41–45]. Note however that in the present case, the presence of typical 4W, 3W, and 2W hydrations states on the same experimental SAXS patterns is rather unusual, for high water contents an homogenous 3W hydration state being commonly reported [11]. We have performed the same experiment at 30% of relative humidity (**Figures S5-S8** and **Videos S6-S7**), showing the same continuous process as well as the coexistence of the 2W and 1W hydration states. Accordingly, the different experiments show a similar trajectory with no influence of surrounding relative humidity but rather a change in overall water content. The coexistence of discrete 4W, 3W, and 2W hydrations states, in addition to nematic contribution, likely reflects a heterogeneous distribution of water content within the droplet.

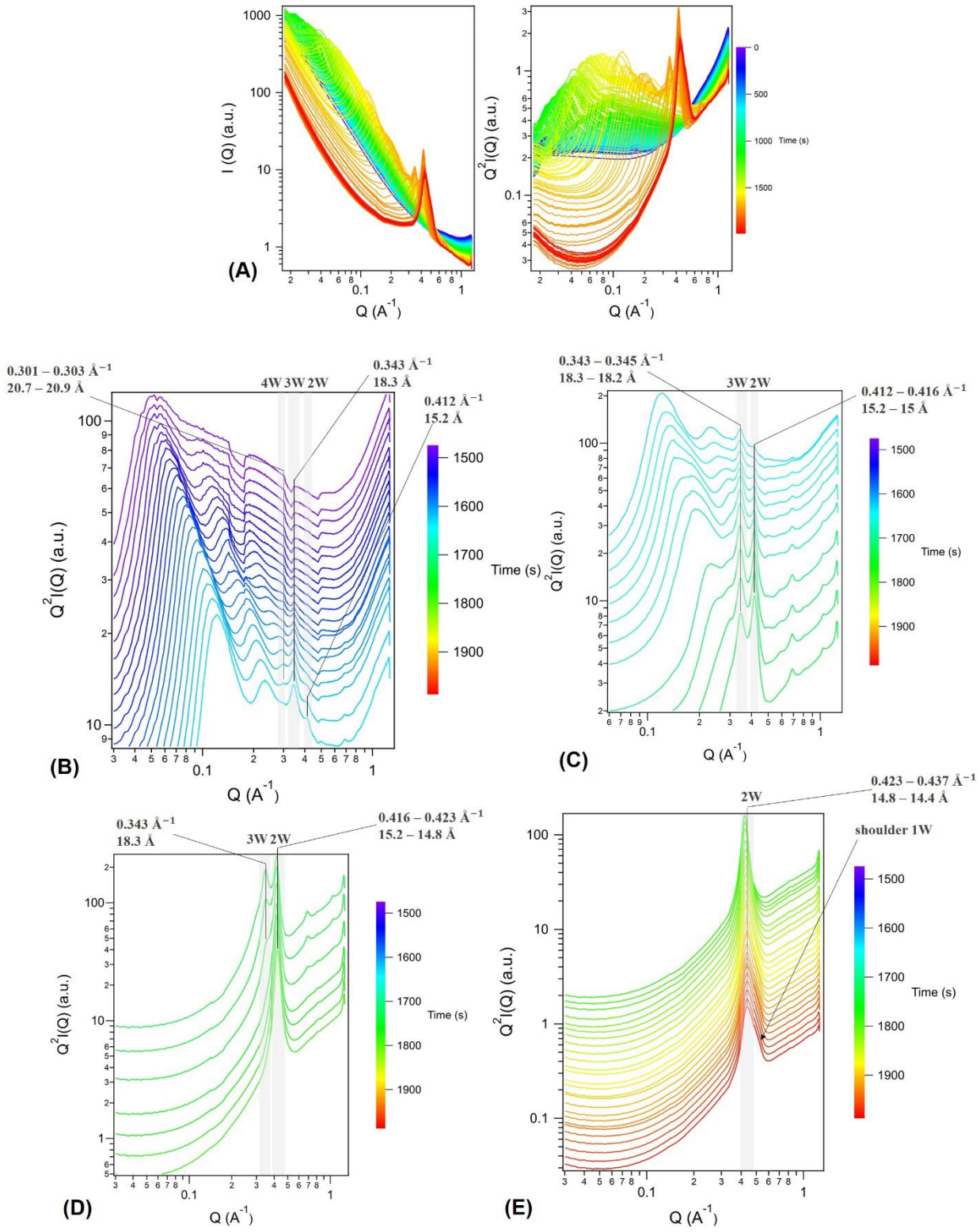

Figure 4. (A) Scattering intensity and structure factor $Q^2I(Q)$ as a function of the scattering vectors Q and as a function of time for 1 µL droplet of SBId-1 ($\Phi_{initial}$ = 0.55%) dried under acoustic levitation at 70% of relative humidity. The curves have been shifted vertically for the sake of

clarity. Structure factor $Q^2I(Q)$ as a function of the scattering vectors Q and as a function of time for 1 µL droplet of SBId-1 ($\Phi_{initial}$ = 0.55%) dried under acoustic levitation at 70% of relative humidity during crystalline compression highlighting the peaks corresponding to **(B)** 4W, 3W and 2W layers; **(C)** 3W and 2W; **(D)** following 3W and 2W; **(E)** 2W and 1W. The curves have been shifted vertically for the sake of clarity.

Modeling of SAXS profiles during crystalline swelling

To derive quantitative information regarding the evolution of the different hydrates in both osmotic and crystalline regime, the sample at $\Phi_{initial}$ = 0.55% was modeled for selected evaporation times with a fitting procedure considering mixed-layer structures (see methods section). The comparison between experimental and calculated patterns is reported in **Figure 5**.

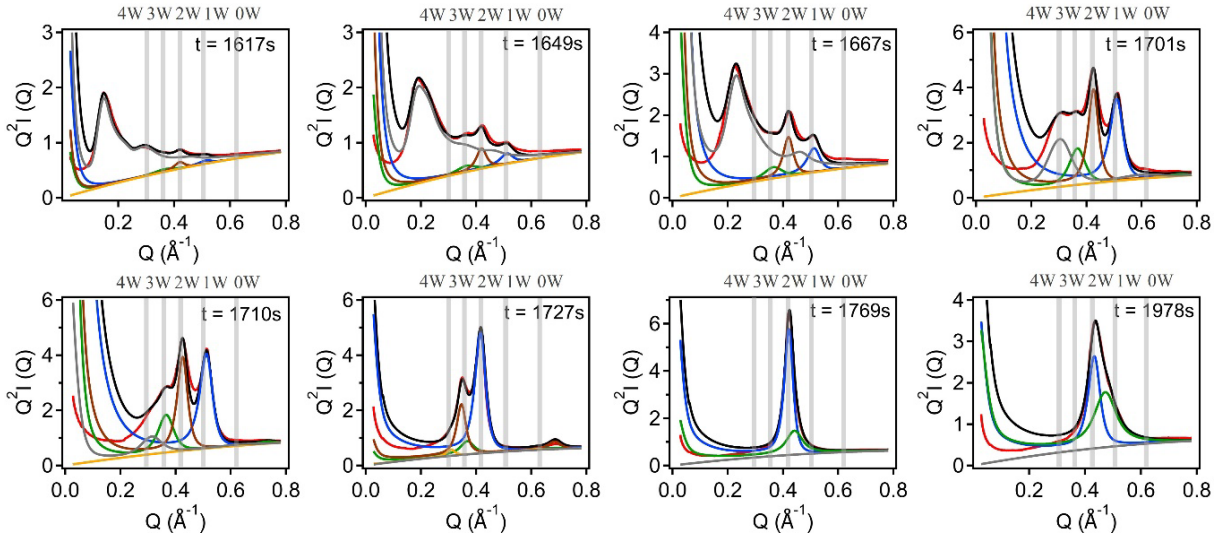

Figure 5. Comparison between experimental (red curves) and calculated $Q^2I(Q)$ SAXS patterns (black curves) including all individual contributions (colored curves) leading to the calculated pattern of the sample at $\Phi_{initial}$ = 0.55% dried under acoustic levitation at 70% of relative humidity for selected evaporation times with a fitting procedure considering mixed-layer structures. Grey rectangles highlight the theoretical peak positions corresponding to 4W, 3W, 2W, 1W and 0W.

The evolution over time during evaporation in relative proportion for the nematic phase and the different hydrates (i.e., 0W, 1W, 2W, 3W, and 4W) is shown in **Figure 6A**. As in the previous section, the average distance between platelets in the nematic phase (*d*n) can be plotted as a function of its relative proportion (**Figure 6B**). The distance decreases until a noticeable change in slope occurs when the system reaches 60% nematic phase and 40% crystalline phase. Beyond this point, the average distance remains relatively constant at ~30 Å, until the nematic phase fully disappears. This indicates that during the drying process, the nematic phase undergoes a contraction to a metastable state at ~30 Å. Interestingly, this mean distance between platelets at ~30 Å is consistent with the pioneer study of Norrish [7] for Na-smectite. This contraction of the nematic phase is followed by a shift towards a saturated crystalline swelling regime, and ultimately progresses to an unsaturated crystalline state. The existence of the 4W, which has been seldom reported in literature in the case of montmorillonite-type of smectite is evidenced here for the first time in the case of beidellite. This 4W hydration state can be fully assigned to the crystalline swelling regime owing to the similar coherent scattering domain size (N=6±0.5) as for other crystalline hydrates, whereas for the nematic phase the number of layers in the stack is significantly decreased (N=2.5). As seen from **Figure 6A**, the crystalline regime follows a continuous process, with the coexistence of the nematic phase alongside 4W, 3W, 2W, 1W, and 0W layers. The final analysis at the end of evaporation indicates the coexistence of 1W and 0W layers that is fully consistent with the final relative humidity reached (i.e., 70% RH).

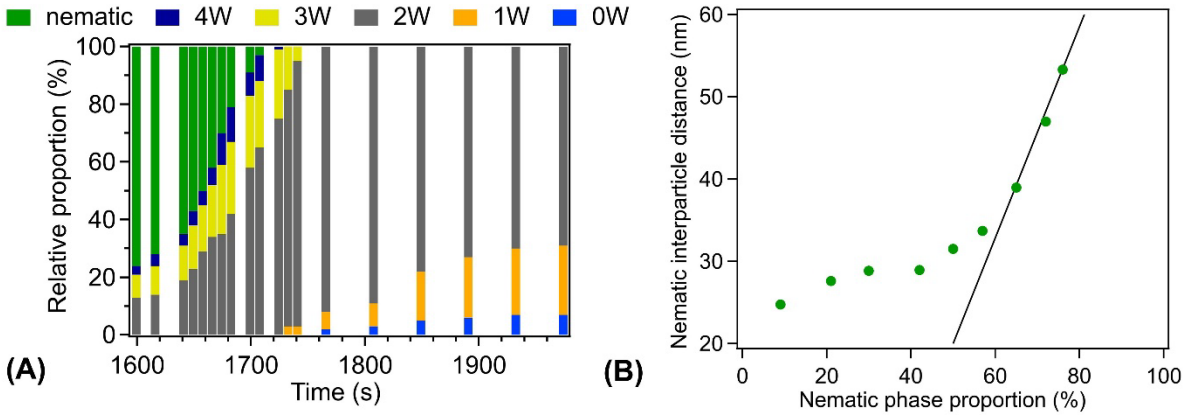

Figure 6. (A) Relative proportion of each hydration states as well as the nematic state as a function of time of evaporation. **(B)** Average distance between platelets in the nematic phase as a function of its relative proportion.

3. Conclusion

In summary, the dehydration mechanism of smectite has been investigated by levSAXS, allowing to probe experimentally and theoretically the linear evolution between the osmotic and the crystalline swelling regime. Upon drying the levitated droplet, we first observe an isotropic to nematic phase transition. This transition is heterogeneous inside the droplet as we observe a splitting of the characteristic nematic peak. The assumption is the occurrence of a faster drying at the edges of the droplet rather than in the "bulk" center. At a certain stage of the drying process, a crystalline state emerges, with a continuous evolution leading to the coexistence of interstratified layers. The process reflects a gradual progression from osmotic swelling to crystalline swelling, characterized by a transition from a pure nematic glass to a coexistence zone where the nematic phase contracts and a saturated crystalline phase emerges, ultimately leading to an unsaturated crystalline state. This transition occurs through a continuous process, where the layer-to-layer space evolves from containing four layers of water (4W) down to 0W, with stratified interlayers.

Methods

Sample preparation. Beidellite (SBId-1) was purchased from the Source Clays Minerals Repository of the Clay Mineral Society at Purdue University, Indiana. The structural formula is $(Si_{7.27}Al_{0.73})(Al_{3.77}Fe^{3+}_{0.11}Mg_{0.21})O_{20}(OH)_4Na_{0.67}$. Details of the sample purification and preparation can be found in Paineau et al. [35]. In this work, we used aqueous dispersions in ultrapure water at three different initial volume fractions ($\Phi_{initial}$ = 0.1, 0.4 and 0.55 %).

Levitation under Small-Angle X-ray Scattering (LevSAXS). Small-Angle X-ray scattering (SAXS) experiments are performed at the SWING beamline, SOLEIL synchrotron (Saint-Aubin, France) using a fixed energy of 12 keV. The scattering patterns are measured with two sample-to-detector distances of 6 m and 0.5 m to access a q-range of 0.0011 $Å^{-1}$ to 0.15 $Å^{-1}$ and 0.12 $Å^{-1}$ to 1.26 $Å^{-1}$, respectively. A commercial acoustic levitator (tec5, 100 kHz free jet nozzle) is implemented on the translation table of the SWING beamline. The setup is equipped with an in-

house humidity regulator based on a proportional integral-derivative (PID) controller adjusting the relative humidity by injecting either dry or water-saturated (compressed air bubbling in pure water) air inside the levitator chamber. Gas flow is insured by two mass-flow meters/controllers (Bronkhorst). For LevSAXS experiments, a droplet of 1 µL of beidellite suspension is placed using a syringe into the acoustic levitator, at a distance of 1.8 mm between the transducer and the reflector while the ultrasonic power level is set at 4 W. The relative humidity is maintained at 70% to ensure the drying of the droplet over one hour. An OAV and its source of white light is used to monitor the dimensions of the droplet throughout the experiment. A MATLAB code is used for determining the volume and the volume fraction of the sample at each step of the evaporation process. Briefly, this code consists of fitting the shape of an ellipse to the droplet contour and to retrieve the lengths of the major a and minor semi axes b of this ellipse. From these data, the volume of the droplet V is determined as $V = \frac{4}{3}\pi * a * a * b$, assuming an axial symmetry around the minor semi axis, and the volume fraction as $\phi = \frac{\phi_{initial} * V_{initial}}{V}$.

SAXS curves modeling. To characterize the different hydration states, the SAXS curves obtained by in-situ measurements at a q-range of 0.12 $Å^{-1}$ to 1.26 $Å^{-1}$ are modeled with a fitting procedure already described in the literature using a trial and error approach [12]. For the crystalline swelling, this procedure considers an interstratified mixed-layer structure that could be composed of up to five discrete states of hydration: dehydrated (0 water sheets, 0W, with layer-to-layer distance at 9.6 Å), 1 (1W at ~12.2 Å), 2 (2W at ~15.1 Å), 3 (3W at ~18.1 Å) and 4 water sheets (4W at ~21.0 Å). The number of mixed-layer structures, the relative proportions of the different types of layers, and the mean number of layers N in the coherent scattering domain size along the c* axis are adjusted to fit the experimental SAXS datas. For all fitted patterns, the N values are 6±0.5 for the different crystalline hydrates. To account for the low-angle region associated to the nematic phase, the strategy of Wilson et al. [43] is also considered. Accordingly, several discrete structures with layer-to-layer distances ranging from 24 to 75 Å, with a step size of 3 Å are first generated, considering a mean number of layers in the coherent scattering domain size N=2.5. This set of obtained XRD patterns were then averaged considering a normal distribution around a mean dn value, representative of mean layer-to-layer distance in the osmotic regime. This value and the relative proportion of the nematic structure relative to the crystalline structures are thus adjusted to reproduce the experimental patterns.

Acknowledgments

This work had benefited from an Investissements d'Avenir grant from Labex PALM (ANR-10-LABX-0039-PALM). The authors would like to thanks the SOLEIL synchrotron for the allocation of beamtime on the SWING beamline under the approved proposal 20230342. We would like to thank the Ellinstru technical team of the Laboratoire de Physique des Solides for the design of the humidity regulator system.

References

[1] F. Bergaya, G. Lagaly, Chapter 1 General Introduction: Clays, Clay Minerals, and Clay Science, in: Dev. Clay Sci., Elsevier, 2006: pp. 1–18. https://doi.org/10.1016/S1572-4352(05)01001-9.

[2] S.W. Bailey, Summary of recommendations of AIPEA nomenclature committee on clay minerals, (n.d.) 7.

[3] F. Bergaya, G. Lagaly, Chapter 2 Structure and Mineralogy of Clay Minerals, in: Dev. Clay Sci., Elsevier, 2006: pp. 21–82. https://doi.org/10.1016/S1572-4352(05)01001-9.

[4] W. Gates, A. Bouazza, G. Churchman, Bentonite clay keeps pollutants at bay., Elements 5 (2009) 105–110. https://doi.org/10.2113/gselements.5.2.105.

[5] X. Liu, C. Tournassat, S. Grangeon, A. Kalinichev, Y. Takahashi, M. Fernandes, Molecular-level understanding of metal ion retention in clay-rich materials, Nat. Rev. Earth Environ. 3 (2022) 1–16. https://doi.org/10.1038/s43017-022-00301-z.

[6] P.F. Luckham, S. Rossi, The colloidal and rheological properties of bentonite suspensions, Adv. Colloid Interface Sci. 82 (1999) 43–92. https://doi.org/10.1016/S0001-8686(99)00005-6.

[7] K. Norrish, The swelling of montmorillonite, Discuss. Faraday Soc. 18 (1954) 120. https://doi.org/10.1039/df9541800120.

[8] V. Dudko, O. Khoruzhenko, S. Weiß, M. Daab, P. Loch, W. Schwieger, J. Breu, Repulsive Osmotic Delamination: 1D Dissolution of 2D Materials, Adv. Mater. Technol. 8 (2023) 2200553. https://doi.org/10.1002/admt.202200553.

[9] W.F. Bradley, R.E. Grim, G.F. Clark, A study of the behavior of montmorillonite upon wetting., Z. Für Krist. 97 (1937) 216–222.

[10] D.M.C. MacEwan, M.J. Wilson, Interlayer and intercalation complexes of clay minerals., Brindley, G.W. and Brown, G., Eds., Crystal Structures of Clay Minerals and Their X-Ray Identification, Mineralogical Society, London, 1980.

[11] B. Dazas, E. Ferrage, A. Delville, B. Lanson, Interlayer structure model of trihydrated low-charge smectite by X-ray diffraction and Monte Carlo modeling in the Grand Canonical ensemble, Am Miner. 99 (2014) 1724–1735.

[12] E. Ferrage, B. Lanson, N. Malikova, A. Plançon, B.A. Sakharov, V.A. Drits, New Insights on the Distribution of Interlayer Water in Bi-Hydrated Smectite from X-ray Diffraction Profile Modeling of 00l Reflections, Chem. Mater. 17 (2005) 3499–3512. https://doi.org/10.1021/cm047995v.

[13] D.A. Laird, Influence of layer charge on swelling of smectites, Layer Charge Clay Miner. 34 (2006) 74–87. https://doi.org/10.1016/j.clay.2006.01.009.

[14] E. Ferrage, Investigation of the Interlayer Organization of Water And Ions in Smectite from the Combined Use of Diffraction Experiments and Molecular Simulations. A Review of Methodology, Applications, and Perspectives, Clays Clay Miner. 64 (2016) 348–373. https://doi.org/10.1346/CCMN.2016.0640401.
[15] M. Holmboe, S. Wold, M. Jonsson, Porosity investigation of compacted bentonite using XRD profile modeling, J. Contam. Hydrol. 128 (2012) 19–32. https://doi.org/10.1016/j.jconhyd.2011.10.005.
[16] S.B. Hendricks, R.A. Nelson, L.T. Alexander, Hydration Mechanism of the Clay Mineral Montmorillonite Saturated with Various Cations1, J. Am. Chem. Soc. 62 (1940) 1457–1464. https://doi.org/10.1021/ja01863a037.
[17] V. Dudko, K. Ottermann, S. Rosenfeldt, G. Papastavrou, J. Breu, Osmotic Delamination: A Forceless Alternative for the Production of Nanosheets Now in Highly Polar and Aprotic Solvents, Langmuir 37 (2021) 461–468. https://doi.org/10.1021/acs.langmuir.0c03113.
[18] J.D.F. Ramsay, S.W. Swanton, J. Bunce, Swelling and dispersion of smectite clay colloids: determination of structure by neutron diffraction and small-angle neutron scattering, J. Chem. Soc. Faraday Trans. 86 (1990) 3919. https://doi.org/10.1039/ft9908603919.
[19] T.A. Egloffstein, Ion exchange in geosynthetic clay liners., Geotech. Fabr. Rep. 15 (1997).
[20] L.J. Michot, I. Bihannic, F. Thomas, B.S. Lartiges, Y. Waldvogel, C. Caillet, J. Thieme, S.S. Funari, P. Levitz, Coagulation of Na-Montmorillonite by Inorganic Cations at Neutral pH. A Combined Transmission X-ray Microscopy, Small Angle and Wide Angle X-ray Scattering Study, Langmuir 29 (2013) 3500–3510. https://doi.org/10.1021/la400245n.
[21] M. Shoaib, S. Khan, O.B. Wani, J. Mata, A.J. Krzysko, I. Kuzmenko, M. Bleuel, L.K. Fiddes, E.W. Roth, E.R. Bobicki, Hybrid microstructure of smectite clay gels revealed using neutron and synchrotron X-ray scattering, Commun. Mater. 4 (2023) 93. https://doi.org/10.1038/s43246-023-00414-y.
[22] C. Baravian, I. Bihannic, P. Davidson, J.F.L. Duval, P. Levitz, S. Maddi, L.J. Michot, E. Paineau, Isotropic/nematic and sol/gel transitions in aqueous suspensions of size selected nontronite NAu1, Clay Miner. 48 (2013) 663–685. https://doi.org/10.1180/claymin.2013.048.5.01.
[23] R. Chaaya, S. Gaboreau, F. Milet, N. Maubec, J. Tremosa, H. Raimbourg, E. Ferrage, In-operando X-ray scattering characterization of smectite swelling experiments, Appl. Clay Sci. 245 (2023) 107124. https://doi.org/10.1016/j.clay.2023.107124.
[24] Q. Shi, W. Di, D. Dong, L.W. Yap, L. Li, D. Zang, W. Cheng, A General Approach to Free-Standing Nanoassemblies *via* Acoustic Levitation Self-Assembly, ACS Nano 13 (2019) 5243–5250. https://doi.org/10.1021/acsnano.8b09628.
[25] D. Zang, Y. Yu, Z. Chen, X. Li, H. Wu, X. Geng, Acoustic levitation of liquid drops: Dynamics, manipulation and phase transitions, Adv. Colloid Interface Sci. 243 (2017) 77–85. https://doi.org/10.1016/j.cis.2017.03.003.
[26] A. Marzo, A. Barnes, B.W. Drinkwater, TinyLev: A multi-emitter single-axis acoustic levitator, Rev. Sci. Instrum. 88 (2017) 085105. https://doi.org/10.1063/1.4989995.
[27] R.H. Morris, E.R. Dye, P. Docker, M.I. Newton, Beyond the Langevin horn: Transducer arrays for the acoustic levitation of liquid drops, Phys. Fluids 31 (2019) 101301. https://doi.org/10.1063/1.5117335.
[28] Y. Liu, M. Agthe, M. Salajková, K. Gordeyeva, V. Guccini, A. Fall, G. Salazar-Alvarez, C. Schütz, L. Bergström, Assembly of cellulose nanocrystals in a levitating drop probed by time-resolved small angle X-ray scattering, Nanoscale 10 (2018) 18113–18118. https://doi.org/10.1039/C8NR05598J.

[29] P. Munier, A. Di, S.E. Hadi, M. Kapuscinski, M. Segad, L. Bergström, Assembly of cellulose nanocrystals and clay nanoplatelets studied by time-resolved X-ray scattering, Soft Matter 17 (2021) 5747–5755. https://doi.org/10.1039/D1SM00251A.
[30] V. Cristiglio, I. Grillo, M. Fomina, F. Wien, E. Shalaev, A. Novikov, S. Brassamin, M. Réfrégiers, J. Pérez, L. Hennet, Combination of acoustic levitation with small angle scattering techniques and synchrotron radiation circular dichroism. Application to the study of protein solutions, Sci. Life – Recent Adv. Biochem. Biophys. Methods 1861 (2017) 3693–3699. https://doi.org/10.1016/j.bbagen.2016.04.026.
[31] C. Hotton, T. Bizien, B. Pansu, C. Hamon, E. Paineau, Evaporation induced self-assembly of imogolite nanotubes in levitation: exploring phase transitions and material shaping, ChemRxiv (2024). https://doi.org/10.26434/chemrxiv-2024-tsfwf.
[32] E. Paineau, K. Antonova, C. Baravian, I. Bihannic, P. Davidson, I. Dozov, M. Impéror-Clerc, P. Levitz, A. Madsen, F. Meneau, L.J. Michot, Liquid-Crystalline Nematic Phase in Aqueous Suspensions of a Disk-Shaped Natural Beidellite Clay, J. Phys. Chem. B 113 (2009) 15858–15869. https://doi.org/10.1021/jp908326y.
[33] E. Paineau, I. Bihannic, C. Baravian, A.-M. Philippe, P. Davidson, P. Levitz, S.S. Funari, C. Rochas, L.J. Michot, Aqueous Suspensions of Natural Swelling Clay Minerals. 1. Structure and Electrostatic Interactions, Langmuir 27 (2011) 5562–5573. https://doi.org/10.1021/la2001255.
[34] L.J. Michot, I. Bihannic, K. Porsch, S. Maddi, C. Baravian, J. Mougel, P. Levitz, Phase Diagrams of Wyoming Na-Montmorillonite Clay. Influence of Particle Anisotropy, Langmuir 20 (2004) 10829–10837. https://doi.org/10.1021/la0489108.
[35] E. Paineau, A.M. Philippe, K. Antonova, I. Bihannic, P. Davidson, I. Dozov, J.C.P. Gabriel, M. Impéror-Clerc, P. Levitz, F. Meneau, L.J. Michot, Liquid–crystalline properties of aqueous suspensions of natural clay nanosheets, Liq. Cryst. Rev. 1 (2013) 110–126. https://doi.org/10.1080/21680396.2013.842130.
[36] P.G. de Gennes, J. Prost, The Physics of Liquid Crystals, Clarendon Press, 1993. https://books.google.fr/books?id=0Nw-dzWz5agC.
[37] J.A.C. Veerman, D. Frenkel, Phase behavior of disklike hard-core mesogens, Phys. Rev. A 45 (1992) 5632–5648. https://doi.org/10.1103/PhysRevA.45.5632.
[38] L. Onsager, The effects of shape on the interaction of colloidal particles, Ann N Acad Sci (1949) 627–659.
[39] C. Baravian, L.J. Michot, E. Paineau, I. Bihannic, P. Davidson, M. Impéror-Clerc, E. Belamie, P. Levitz, An effective geometrical approach to the structure of colloidal suspensions of very anisometric particles, EPL Europhys. Lett. 90 (2010) 36005. https://doi.org/10.1209/0295-5075/90/36005.
[40] J.D.F. Ramsay, S.W. Swanton, J. Bunce, Swelling and dispersion of smectite clay colloids: determination of structure by neutron diffraction and small-angle neutron scattering, J. Chem. Soc. Faraday Trans. 86 (1990) 3919. https://doi.org/10.1039/ft9908603919.
[41] K. Devineau, I. Bihannic, L. Michot, F. Villiéras, F. Masrouri, O. Cuisinier, G. Fragneto, N. Michau, In situ neutron diffraction analysis of the influence of geometric confinement on crystalline swelling of montmorillonite, Appl. Clay Sci. 31 (2006) 76–84. https://doi.org/10.1016/j.clay.2005.08.006.
[42] A. Fernández, Fernández, A.M[a]., Rivas, P., 2005a. Analysis and distribution of waters in the compacted FEBEX bentonite: pore water chemistry and adsorbed water properties. In: Alonso, E.E., Ledesma, A. (Eds.), Advances in Understanding Engineered Clay Barriers. AA Balkema Publishers, Leiden, pp. 257–275., in: 2005: pp. 257–275.

[43] J. Wilson, J. Cuadros, G. Cressey, An In situ Time-Resolved XRD-PSD Investigation into Na-Montmorillonite Interlayer and Particle Rearrangement during Dehydration, Clays Clay Miner. 52 (2004) 180–191. https://doi.org/10.1346/CCMN.2004.0520204.
[44] E. Ferrage, B. Lanson, B. Sakharov, V. Drits, Investigation of smectite hydration properties by modeling experimental X-ray diffraction patterns: Part I. Montmorillonite hydration properties, Am. Mineral. 90 (2005) 1358–1374. https://doi.org/10.2138/am.2005.1776.
[45] E. Ferrage, B. Lanson, B.A. Sakharov, N. Geoffroy, E. Jacquot, V.A. Drits, Investigation of dioctahedral smectite hydration properties by modeling of X-ray diffraction profiles: Influence of layer charge and charge location, 92 (2007) 1731–1743. https://doi.org/10.2138/am.2007.2273.